Performance Evaluation of Titanium Ion Optics for the NASA 30 cm Ion Thruster*†

George C. Soulas
NASA Glenn Research Center
M.S. 301-3
21000 Brookpark Road
Cleveland, OH 44135, U.S.A.
216-977-7419
George.C.Soulas@grc.nasa.gov

IEPC-01-092

The results of performance tests with titanium ion optics were presented and compared to those of molybdenum ion optics. Both titanium and molybdenum ion optics were initially operated until ion optics performance parameters achieved steady state values. Afterwards, performance characterizations were conducted. This permitted proper performance comparisons of titanium and molybdenum ion optics. Ion optics' performance was characterized over a broad thruster input power range of 0.5 to 3.0 kW. All performance parameters for titanium ion optics of achieved steady state values after processing 1200 gm of propellant. Molybdenum ion optics exhibited no burn-in. Impingement-limited total voltages for titanium ion optics were up to 55 V greater than those for molybdenum ion optics. Comparisons of electron backstreaming limits as a function of peak beam current density for molybdenum and titanium ion optics demonstrated that titanium ion optics operated with a higher electron backstreaming limit than molybdenum ion optics for a given peak beam current density. Screen grid ion transparencies for titanium ion optics were as much as 3.8% lower than those for molybdenum ion optics. Beam divergence half-angles that enclosed 95% of the total beam current for titanium ion optics were within 1-3º of those for molybdenum ion optics. All beam divergence thrust correction factors for titanium ion optics were within 1% of those with molybdenum ion optics.

Introduction

The NSTAR (i.e. NASA Solar Electric Propulsion Technology Applications Readiness Program) 30 cm ion thruster system on the Deep Space 1 mission has demonstrated the viability of ion propulsion for deep space missions.[1,2] Ion propulsion is, therefore, a candidate for several deep space missions, such as the Neptune Orbiter, Titan Explorer, Mars Sample Return, Europa Lander, and others. However, ion propulsion system mass and volume could be significantly reduced for many of these missions by increasing the NSTAR thruster's propellant throughput and peak input power capabilities beyond that already demonstrated by past and ongoing wear tests.[3,4] Propulsion system mass and volume reductions occur because fewer thrusters and, therefore, fewer accompanying power processors and propellant feed system components, would be required.

Increasing propellant throughput and thruster power is limited, in part, by charge-exchange sputter erosion of the accelerator grid.[5,6] Significant charge-exchange accelerator grid sputter erosion can lead to electron backstreaming due to accelerator aperture enlargement, grid structural failure due to pit and groove erosion of the downstream surface, and an unclearable grid short by a flake from sputter-eroded

* Presented as Paper IEPC-01-092 at the 27th International Electric Propulsion Conference, Pasadena, CA, 15-19 October, 2001.

accelerator grid material.[6] Utilizing an ion optics material with a lower volumetric sputter erosion rate addresses all of the aforementioned failure mechanisms to extend propellant throughput and increase thruster power density.

A development effort was initiated at the NASA Glenn Research Center (GRC) to identify a material with a lower accelerator grid volumetric sputter erosion rate than molybdenum (i.e. the present NSTAR thruster grid material). Such an activity could utilize NSTAR thruster grid design and fabrication techniques to keep development costs low.[7,8] Titanium was found to offer a 45% reduction in volumetric erosion rates and could be fabricated using the same fabrication techniques as molybdenum ion optics. Accelerator grid life was expected to improve by a factor of 1.9x.

Several titanium grid sets were successfully fabricated and performance tested with NSTAR 30 cm engineering model ion thrusters. Titanium ion optics were successfully operated over an extended power range of 0.5 to 4.6 kW. Ion optics performance parameters that included impingement-limited total voltages, electron backstreaming limits, screen grid ion transparencies, and beam divergence were compared to those of molybdenum ion optics. However, these performance parameters were found to be changing rapidly with accumulated operating time.[8] This initial rapid change in ion optics' performance, referred to as an ion optics burn-in in this report, was speculated to have been due to small initial changes in either accelerator grid aperture diameters from sputter erosion or grid hot gap from stress-relieving of the domed material. This burn-in phenomenon has been noted with molybdenum ion optics during an NSTAR long duration test.[4]

Because performance parameters from these prior titanium ion optics tests had not yet achieved steady state values, a proper one-to-one performance comparison with molybdenum ion optics could not be completed. An investigation was, therefore, initiated to burn-in titanium ion optics by operating them until ion optics performance parameters achieved steady state values. Afterwards, ion optics' performance was determined. The same was done for a molybdenum ion optics set, and the performance of these two materials was compared. Ion optics' performance was characterized over a broad thruster input power range of 0.5 to 3.0 kW. This paper reports on the results of these tests.

Test Hardware and Operating Procedures

Titanium Ion Optics

A photograph of 30 cm titanium grids is shown in Fig. 1. The titanium ion optics set utilized for this investigation was set B of Ref. [8]. Screen and accelerator grid aperture diameter variations were within +0%/-9% and ±9%, respectively, of the nominal NSTAR design throughout the active area.[9,10] In general, accelerator grid aperture diameters were lower-than-nominal at the active area center while screen grid aperture diameters were lower-than-nominal at the active area perimeter. The resulting screen grid open area in the active area perimeter fraction was estimated to be 10-13% lower-than-nominal. Grid cold gap variations throughout the active area were within +4%/–0% of the nominal NSTAR design, which was better than the variations for the molybdenum ion optics used for these tests. The screen grid thickness was also 7% thicker than the nominal NSTAR design. Although this grid set had bonded together due to temperature differences between the grids during thruster start-up on a prior test, the grids were subsequently separated, and aperture alignment and cold grid gap changes were found to be negligible.[8] Thruster start-up procedures were modified to preclude this from occurring and will be discussed in a later section.

Molybdenum Ion Optics

Molybdenum ion optics fabricated at NASA GRC were also tested to provide a baseline performance for comparison. These ion optics were the same as those used in Ref. [8]. Screen and accelerator grid aperture diameter variations were within +0%/–3% and ±4%, respectively, of the nominal NSTAR design throughout the active area.[9,10] Accelerator grid aperture diameters were larger-than-nominal at the active area center while screen grid aperture diameters were lower-than-nominal at the active area perimeter. The resulting screen grid open area in the active area perimeter fraction was estimated to be only 3-4% lower-than-nominal. Grid cold gap variations throughout the active area were within ±8% of the nominal NSTAR design.

Ion Thruster
Both ion optics sets were mounted onto a 30 cm ion thruster, shown in Fig. 2, which was the same thruster as that reported in Ref. [8]. This thruster serves as a test bed for 30 cm thruster development at NASA.[11] The mechanical designs of the thruster discharge chamber and ion optics are nearly identical to those of the NSTAR thruster, described in detail in Refs. [9] and [10]. The thruster was fitted with thermocouples for thermal tests and the exterior was modified so that a second neutralizer could be installed.

Power Console and Gas Feed System
A power console similar to that described in Ref. [12] powered the thruster. This power console was modified to allow the thruster to be throttled up to 5 kW. A high purity gas feed system was used to provide xenon to the discharge cathode, discharge chamber, and neutralizer through separate mass flow controllers.

Diagnostics
During thruster operation, voltages and currents were measured with digital multimeters and xenon flows with mass flow meters. These measured parameters were used to set thruster operating conditions, as well as to determine thruster performance.

The thruster was connected to an electrically floating power supply circuit used to determine the screen grid transparency to discharge chamber ions. The circuit electrically tied the screen grid to the discharge cathode during normal operation, but biased the grid negative relative to discharge cathode potential to repel electrons and measure the collected ion current.

Beam current density profiles were measured with a probe mounted onto a two-axis probe motion system. The probe was a planar geometry with a 1.0 cm^2 circular current-collecting area.[13] The probe was biased negative with respect to beam plasma potential to repel electrons and was grounded through a resistor that acted as a shunt to measure collected currents.

The positioning system swept the probe in the radial and axial directions through the vertical center of the thruster ion optics. The positioning system had a 1.25 m maximum travel in each axis, which enabled near-field radial beam current density measurements at different axial locations, as measured from the geometric center of the ion optics. The current density measurements were then used to determine beam current density profiles, beam divergence half-angles, and thrust correction factors.[8]

Vacuum Facility
Testing was conducted in Vacuum Facility 11 at NASA GRC. This 2.2 m diameter × 7.9 m long facility is evacuated with seven cryogenic pumps and a turbomolecular pump. The total measured facility pumping speed was greater than 100,000 l/s with xenon. The facility base pressure was typically less than 2.6×10^{-5} Pa (2×10^{-7} Torr) and background pressures were as high as 5.2×10^{-4} Pa (3.9×10^{-6} Torr) at the peak thruster input power of 3.0 kW.

Ion Optics Performance Parameters
Ion optics performance parameters were determined throughout testing. These parameters included impingement-limited total voltages, electron backstreaming limits, screen grid ion transparencies, accelerator grid currents, beam divergence, and beam divergence thrust losses.

Impingement-limited total voltages were determined from plots of accelerator current as a function of total voltage where the slope was -0.02 mA/V. Total voltage is the sum of the absolute values of the beam and accelerator power supply voltages. Perveance margins were defined as the difference between the total voltage during normal operation (i.e. the settings defined in Table 1) and the impingement-limited total voltage. Uncertainties in impingement-limited total voltage determinations (and, therefore, perveance margins) were within ±10 V.

The electron backstreaming limit was determined by lowering the magnitude of the accelerator grid voltage until the indicated beam current increased by 0.1 mA due to backstreaming electrons. Uncertainties in electron backstreaming limit measurements were estimated to be within ±1 V.

Screen grid ion transparencies were determined by biasing the screen grid 20 V below discharge cathode potential to repel electrons and to measure the collected ion current. The method used to determine screen grid ion transparency from these measurements is discussed in detail in Ref. [8]. Uncertainties in screen grid ion transparency measurements were estimated to be within ±0.002.

Radial beam current density profiles were used to determine beam divergence and thrust loss, and to provide peak current densities for comparisons of electron backstreaming limits, which will be discussed in a later section. Regarding beam current density measurements, no attempt was made to repel charge-exchange ions from the probe or to account for secondary electron emission due to ion bombardment. Integration of the radial beam current density profiles (assuming azimuthal symmetry) yielded beam currents that were higher than the measured beam current by as much as 15%. It is anticipated that these errors were caused by a combination of effects, which included the large probe surface area, measurement of charge-exchange ions in the beam, secondary electron emission from both singly- and doubly-charged ions, and a slightly asymmetric beam.

Radial beam current density profiles were taken at five axial locations to determine beam divergence half-angles and thrust losses due to beam divergence. The methods used to determine divergence half-angles and thrust losses are discussed in detail in Ref. [8]. Uncertainties in the beam divergence half-angles and beam divergence thrust losses due to beam divergence cannot presently be assessed due to the unknown sources of error in the beam current density measurements.

Operating Procedures

Molybdenum and titanium ion optics were tested on the 30 cm ion thruster at the thruster input power levels and corresponding operating parameters listed in Table 1. These power levels included NSTAR operating points that encompassed the full 0.5-2.3 kW throttling range,[14] as well as operating points with a higher beam voltage for operation up to 3.0 kW. During thruster operation, main and discharge cathode flows were maintained at fixed values while the discharge current was adjusted to maintain a constant beam current.

During each test, the ion optics were initially operated for an extended duration to allow ion optics performance parameters to achieve steady state values. The thruster was operated primarily at the TH15 operating point (see Table 1) while monitoring changes in impingement-limited total voltages, electron backstreaming limits, screen grid ion transparencies, and radial beam current density profiles. The thruster was not operated continuously, but was intentionally interrupted on several occasions. When these ion optics performance parameters had achieved steady state values, the thruster was step-ramped through operating points listed in Table 1 to characterize ion optics' performance. At each operating point, ion optics performance parameters such as impingement-limited total voltages, electron backstreaming limits, screen grid ion transparencies, and beam current density profiles, as well as other thruster performance parameters, were determined. Upon completion of each ion optics' performance data sets, the ion optics were re-characterized at TH15 to confirm that ion optics' performance had not changed.

Prior titanium ion optics tests had revealed that 30 cm titanium ion optics can make contact and bond together if beam extraction is initiated immediately following discharge ignition.[8] This was speculated to have been due to the initial uneven temperatures of the grids during thruster startup from room temperature. This issue was overcome in this investigation by merely allowing the discharge chamber to heat the ion optics for a minimum of 20 minutes prior to initiating beam extraction. This duration is conservative, however, since temporal electron backstreaming measurements from room temperature to TH15 have indicated that beam extraction may have been initiated as soon as 10 minutes following ignition.[7]

Results and Discussions

Ion Optics Burn-in

The results of ion optics burn-in at TH15 for both grid materials are plotted in Fig. 3. Performance parameters were plotted as a function of propellant throughput and not accumulated operation because the ion optics were operated at several different power levels during these burn-in periods. Monitored ion optics performance parameters included perveance margin, electron backstreaming limit, screen grid ion transparency, and beam current density profiles.

Titanium Ion Optics

For the titanium ion optics, the performance parameters of Fig. 3 achieved steady state values at different propellant throughputs. Perveance margins achieved steady state at about 750 gm, then electron backstreaming limits at about 1030 gm, and finally screen grid ion transparencies at about 1200 gm. Perveance margins and screen grid ion transparencies generally increased during the first 400 gm of

propellant throughput, and decreased thereafter until steady state values were reached. Electron backstreaming limits generally increased after the first 400 gm of propellant throughput.

Radial beam current density profiles at various propellant throughputs are plotted in Fig. 4 after 400 gm of propellant throughput. The profiles show that although the peak beam current density did not change significantly, the beam current densities increased at radii of –100 mm to –20 mm and 20 mm to 100 mm. Specifically, positive radial locations showed a steady increase in beam current density until 1205 gm of propellant throughput, while negative radial locations increased only until 705 gm of propellant throughput. These changes, however, were small.

Although the post-test cold grid gap was measured to be 0% to +8% of the pre-test gap at the outer-radius, mid-radius, and center of the grid active area, this change was also within the accuracy of the measurement. Post-test accelerator aperture diameters showed little or no change at the active area outer- and mid-radii, but increased by 2-5% within 5-10 mm of the active area center.

Trends for each performance parameter changed at about 400 gm of propellant throughput. This may be related to the grids making contact and bonding together at 193 gm of propellant throughput, however, this cannot be confirmed.[8] The increasing perveance margin prior to 400 gm of propellant throughput may have been due to the increased accelerator aperture diameters at the active area center, where beam current per hole is highest. The changes after 400 gm in all monitored performance parameters are consistent with an increasing grid hot gap, especially at the geometric center of the grid active area. An increasing hot grid gap decreases perveance margins and increases in electron backstreaming limit magnitudes.[15] A larger hot grid gap is also known to increase discharge losses by reducing screen grid ion transparency.[16] The changes in the cold grid gap, however, were too small to confirm this change. Furthermore, it is presently unclear how this speculated hot gap increase may have contributed to the changes in the radial beam current density profiles. Regardless, all ion optics performance parameters achieved steady state values by 1200 gm of propellant throughput. Titanium ion optics' performance characterization results presented in the remainder of this paper were measured following this point. As shown in Fig. 3, the aforementioned ion optics performance parameters did not change following performance characterizations.

Molybdenum Ion Optics

The results for molybdenum ion optics shown in Fig. 3 showed no significant changes in any of these performance parameters. If a burn-in had occurred for this ion optics set, it would have to have occurred prior to a propellant throughput of 230 gm. Ion optics' performance characterizations were initiated at 570 gm of propellant throughput. Following performance characterizations, Fig. 3 shows that although perveance margins and electron backstreaming limit remained unchanged, the screen grid ion transparency had decreased by 0.8% for unknown reasons.

Burn-in has been noted with molybdenum ion optics during an NSTAR thruster long duration test.[4] Rapid decreases in perveance margins, screen grid ion transparencies, and electron backstreaming limit magnitudes were noted within the first 150 hours, or 1.3 kg of xenon, of life testing. These changes are consistent with an increasing grid hot gap.

Impingement-Limited Total Voltage

Beam current as a function of impingement-limited total voltage is plotted in Fig. 5 for titanium and molybdenum ion optics. Perveance margins for titanium ion optics are listed in Table 2 with results from molybdenum ion optics for comparison.

As Fig. 5 and Table 2 demonstrate, impingement-limited total voltages for titanium ion optics were about 45-55 V greater than those of molybdenum ion optics at the highest beam current. This disparity decreased to 10-15 V for the lowest beam current. The difference between the two grid materials was due to the larger beam current densities at the active area center for the titanium ion optics (presented in a later section). This is demonstrated in Fig. 6, where the peak beam current density is plotted as a function of impingement-limited total voltage for titanium and molybdenum ion optics. The larger beam current densities at the active area center of the titanium ion optics were the result of higher beam currents per hole in this region, which caused higher impingement-limited voltages. Regardless, the agreement in perveance margin shown in Table 2 is considered sufficient because there is adequate margin at all operating points in Table 1. Furthermore,

impingement-limited total voltages are known to decrease with thruster operation.[3]

Electron Backstreaming Limit

Electron backstreaming limit voltages for the titanium ion optics are listed in Table 2 with results with molybdenum ion optics for comparison. Since the electron backstreaming limit is also a function of the peak beam current density,[8] the electron backstreaming limit is plotted as a function of the peak beam current density (listed in Table 3) in Fig. 6 for a more appropriate comparison. The data for each grid set are presented at separate beam voltages because the electron backstreaming limit is also a function of beam voltage.[15]

Table 2 shows that the electron backstreaming limits of titanium ion optics were 1-7 V higher than those of molybdenum ion optics. However, peak beam current densities, listed in Table 3, were also 0.1-0.5 mA/cm^2 higher than those for molybdenum ion optics. Fig. 7, which correlates both parameters, demonstrates that titanium ion optics operated with a higher electron backstreaming limit than molybdenum ion optics for a given peak beam current density. This disparity, though small, is speculated to have been due, in part, to the larger-than-nominal accelerator aperture diameters for the molybdenum ion optics and lower-than-nominal accelerator aperture diameters for the titanium ion optics at the active area center. The electron backstreaming limit decreases with increasing accelerator aperture diameter.[15]

Screen Grid Ion Transparency

Table 3 lists screen grid ion transparencies for titanium ion optics with results from molybdenum ion optics for comparison. Screen grid ion transparencies for titanium ion optics were as much as 3.8% lower than those for molybdenum ion optics. This reflected the smaller physical open area fraction of the titanium ion optics' screen grid at the perimeter of the active area and slightly thicker titanium screen grid.

Accelerator Current

Table 3 lists accelerator currents for titanium ion optics with results from molybdenum ion optics for comparison. Accelerator currents for titanium ion optics were within 4% of those for molybdenum ion optics.

Beam Current Density Profiles, Beam Divergence, and Thrust Loss

Sample radial beam current density distributions for both grid materials are shown in Fig. 8, taken 48 mm downstream of the grid center. Radial beam current density distributions at several axial locations are shown in Fig. 9 for titanium ion optics. Peak beam current densities were determined from radial beam current density profiles taken 48 mm downstream of the grid center. Table 3 lists peak beam current densities for titanium ion optics with results from molybdenum ion optics for comparison. As Table 3 shows, peak beam current densities for titanium ion optics were 4-8% higher than those for molybdenum ion optics. It is speculated that the larger peak beam current densities for titanium ion optics was due to the smaller screen grid aperture diameters at the perimeter of the active area. This reduced the physical open area fraction in this region, requiring a higher discharge plasma density to provide the required beam current. This caused more ion current to be extracted through the center of the active area. This higher discharge plasma density was reflected in the 2-5% higher discharge losses for the titanium ion optics, as shown in Table 3. It is noteworthy that the larger peak beam current densities for titanium ion optics likely contributed to the lower screen grid ion transparencies and higher impingement-limited total voltage, as discussed in earlier sections.

Figures 8 and 9 also show that beam current density profiles were slightly non-axisymmetric near the active area center for both ion optics materials. This slight asymmetry occurred at all power levels tested and is an artifact of the thruster discharge chamber plasma.[8]

Beam divergence angles that enclosed 95% of the total beam current are listed in Table 4 for titanium ion optics with results from molybdenum ion optics for comparison. Divergence half-angle data for the titanium ion optics were within 1-3º of those for the molybdenum ion optics. Sample plots of percentage of total beam current that enclosed a given divergence half-angle are shown in Fig. 10 for titanium and molybdenum ion optics. Beam divergence half-angles were almost identical for both ion optics materials.

Table 4 lists these thrust correction factors due to beam divergence for titanium ion optics with results from molybdenum ion optics for comparison. All

values for titanium ion optics were within 1% of those with molybdenum ion optics. This close agreement demonstrates that thrust losses from beam divergence are very similar for titanium and molybdenum ion optics.

Conclusions

The results of performance tests with titanium and molybdenum ion optics were presented. Both titanium and molybdenum ion optics were initially operated until ion optics performance parameters achieved steady state values. Afterwards, performance characterizations were conducted. This permitted proper performance comparisons of titanium and molybdenum ion optics over a broad thruster input power range of 0.5 to 3.0 kW.

All performance parameters for titanium ion optics achieved steady state values after processing 1200 gm of propellant. Trends for each performance parameter changed at about 400 gm of propellant throughput. Changes in performance parameters after 400 gm are consistent with an increasing grid hot gap, especially at the geometric center of the grid active area. Unfortunately, changes in the cold grid gap were too small to confirm this change. Molybdenum ion optics exhibited no burn-in.

Impingement-limited total voltages for titanium ion optics were about 45-55 V greater than those of molybdenum ion optics at the highest beam currents. This disparity decreased to 10 V for the lower beam currents. The difference between the two grid materials was due to the larger beam current densities at the active area center for the titanium ion optics. This agreement is considered sufficient because there was adequate perveance margin at all operating points.

Comparisons of electron backstreaming limits as a function of peak beam current density for molybdenum and titanium ion optics demonstrated that titanium ion optics operated with a higher electron backstreaming limit than molybdenum ion optics for a given peak beam current density. This disparity is speculated to have been due, in part, to the larger-than-nominal accelerator aperture diameters for the molybdenum ion optics and lower-than-nominal accelerator aperture diameters for the titanium ion optics at the active area center.

Screen grid ion transparencies for titanium ion optics were up to 3.8% lower than those for molybdenum ion optics, reflecting the smaller physical open area fraction of the titanium ion optics' screen grid at the perimeter of the active area and slightly thicker titanium screen grid.

Beam divergence half-angles that enclosed 95% of the total beam current for titanium ion optics were within 1-3º of those for molybdenum ion optics. All beam divergence thrust correction factors for the titanium ion optics were within 1% of those for the molybdenum ion optics.

References

[1] Rawlin, V.K., et al. "An Ion Propulsion System for NASA's Deep Space Missions," AIAA Paper 99-4612, September 1999.

[2] Polk, J.E., et al., "In-Flight Performance of the NSTAR Ion Propulsion System on the Deep Space One Mission," IEEE Aerospace Conference Paper 8.0304, March 2000.

[3] Polk, J.E., et al., "An Overview of the Results from an 8200 Hour Wear Test of the NSTAR Ion Thruster," AIAA Paper 99-2446, June 1999.

[4] Anderson, J.R., et al., "Performance Characteristics of the NSTAR Ion Thruster During an On-going Long Duration Ground Test," IEEE Aerospace Conference Paper 8.0303, March 2000.

[5] Rawlin, V.K., "Erosion Characteristics of Two-Grid Ion Accelerating Systems," IEPC Paper 93-175, September 1993.

[6] Brophy, J.R., Polk, J.E., and Rawlin, V.K., "Ion Engine Service Life Validation by Analysis and Testing," AIAA Paper 96-2715, July 1996.

[7] Soulas, G.C., Haag, T.W., Patterson, M.J., and Rawlin, V.K., "Titanium Optics for Ion Thrusters," IEPC Paper 99-149, October 1999.

[8] Soulas, G.C., "Performance of Titanium Optics on a NASA 30 cm Ion Thruster," AIAA Paper 2000-3814, July 2000.

[9] Christensen, J.A., et al., "Design and Fabrication of a Flight Model 2.3 kW Ion Thruster for the Deep Space 1 Mission," AIAA Paper 98-3327, July 1998.

[10] Sovey, J.S., et al., "Development of an Ion Thruster and Power Processor for New Millenium's Deep Space 1 Mission," AIAA Paper 97-2778, December 1997.

[11] Patterson, M.J., et al., "Ion Propulsion Development Activities at NASA Glenn Research Center," AIAA Paper 2000-3810, July 2000.

[12] Pinero, L.R., Patterson, M.J., and Satterwhite, V.E., "Power Console Development for NASA's Electric Propulsion Outreach Program," IEPC Paper 93-250, September 1993.

[13] Foster, J.E., Soulas, G.C., and Patterson, M.J., "Plume and Discharge Plasma Measurements of a 5 kW NSTAR-Derivative Ion Thruster," AIAA Paper 2000-3812, July 2000.

[14] Rawlin, V.K., et al., "NSTAR Flight Thruster Qualification Testing," AIAA Paper 98-3936, July 1998.

[15] Kaufman, H.R., "Technology of Electron Bombardment Ion Thrusters," Advances in Electronics and Electron Physics, vol. 36, Academic Press, Inc., New York, 1974, pp. 265-373.

[16] Rawlin, V.K., "Performance of 30-cm Ion Thrusters with Dished Accelerator Grids," AIAA Paper 73-1053," October-November 1973.

Table 1. Nominal thruster operating parameters.

Power Level Designation	Input Power,[a] kW	Beam Current,[b] A	Beam Voltage,[b] V	Accelerator Voltage, V	Neutralizer Keeper Current, A	Main Flow, sccm	Discharge Cathode Flow, sccm	Neutralizer Flow, sccm
TH0[c]	0.5	0.51	650	-150	2.0	5.98	2.47	2.40
TH4[c]	1.0	0.71	1100	-150	2.0	8.30	2.47	2.40
TH8[c]	1.4	1.10	1100	-180	1.5	14.4	2.47	2.40
TH10[c]	1.7	1.30	1100	-180	1.5	17.2	2.56	2.49
TH12[c]	1.8	1.49	1100	-180	1.5	18.5	2.72	2.65
TH15[c]	2.3	1.76	1100	-180	1.5	23.4	3.70	3.60
THe4	0.6	0.56	1500	-250	2.0	6.50	2.47	2.40
THe8	0.8	0.85	1500	-250	2.0	10.6	2.47	2.40
THe11	1.1	1.06	1500	-250	2.0	14.0	2.47	2.40
THe14	1.3	1.27	1500	-250	1.5	17.0	2.56	2.46
THe16	2.5	1.44	1500	-250	1.5	19.2	2.81	2.72
THe19	3.0	1.76	1500	-250	1.5	23.1	3.54	3.60

[a]Nominal values.
[b]Power supply current or voltage.
[c]Nominal NSTAR operating condition.

Table 2. Perveance margins and electron backstreaming limits for titanium and molybdenum ion optics.

Power Level Designation	Perveance Margin, V		Electron Backstreaming Limit, V	
	Ti	Mo	Ti	Mo
TH0[a]	165	175	-70	-69
TH4[a]	515	540	-124	-126
TH8[a]	425	455	-137	-138
TH10[a]	370	405	-141	-143
TH12[a]	325	365	-144	-148
TH15[a]	240	295	-149	-156
THe4	1090	1105	-142	-145
THe8	970	1000	-167	-171
THe11	910	940	-180	-181
THe14	850	885	-184	-183
THe16	-	845	-	-189
THe19	715	760	-192	-197

[a]Nominal NSTAR operating condition.

Table 3. Peak beam current densities, screen grid ion transparencies, discharge losses, and accelerator currents for titanium and molybdenum ion optics.

Power Level Designation	Peak Beam Current Densities,[a] mA/cm^2		Screen Grid Ion Transparencies		Discharge Losses, W/A		Accelerator Currents, mA	
	Ti	Mo	Ti	Mo	Ti	Mo	Ti	Mo
TH0[b]	2.5	2.4	0.827	0.836	250	250	1.4	1.4
TH4[b]	3.4	3.2	0.872	0.882	250	240	1.8	1.8
TH8[b]	4.6	4.3	0.864	0.877	200	200	3.5	3.5
TH10[b]	5.2	4.8	0.854	0.870	197	191	4.6	4.5
TH12[b]	5.6	5.3	0.843	0.863	194	187	5.7	5.5
TH15[b]	6.2	5.8	0.818	0.849	197	188	7.5	7.2
THe4	2.8	2.6	0.904	0.912	233	225	1.5	1.5
THe8	3.8	3.7	0.906	0.909	200	200	2.6	2.5
THe11	4.5	4.3	0.904	0.913	190	190	3.5	3.5
THe14	5.1	4.8	0.898	0.908	190	180	4.2	4.4
THe16	-	5.3	-	0.904	-	179	-	5.1
THe19	6.3	6.0	0.875	0.895	185	178	6.6	6.8

[a]Peak beam current densities at 48 mm downstream of the geometric center of the ion optics; peak beam current densities occurred at approximately the radial center of the grid active area.
[b]Nominal NSTAR operating condition.

Table 4. Divergence half-angles that enclosed 95% of total beam current and beam divergence thrust correction factors for titanium and molybdenum ion optics.

Power Level Designation	Divergence Half-angle at 95% of Beam Current, degrees		Thrust Correction Factor for Beam Divergence	
	Ti	Mo	Ti	Mo
TH0[a]	28	29	0.97	0.97
TH4[a]	-	29	-	0.97
TH8[a]	28	29	0.97	0.97
TH10[a]	27	28	0.98	0.97
TH12[a]	-	27	-	0.98
TH15[a]	25	26	0.98	0.98
THe4	32	29	0.96	0.96
THe8	-	29	-	0.96
THe11	-	29	-	0.97
THe14	-	29	-	0.97
THe16	-	29	-	0.97
THe19	29	29	0.97	0.97

[a]Nominal NSTAR operating condition.

Fig. 1. Photograph of titanium grids with and without the ion optics mounting ring.

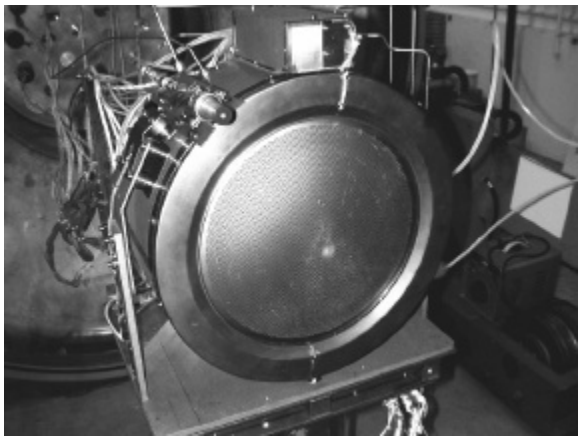

Fig. 2. Titanium ion optics installed onto a NASA 30 cm ion thruster.

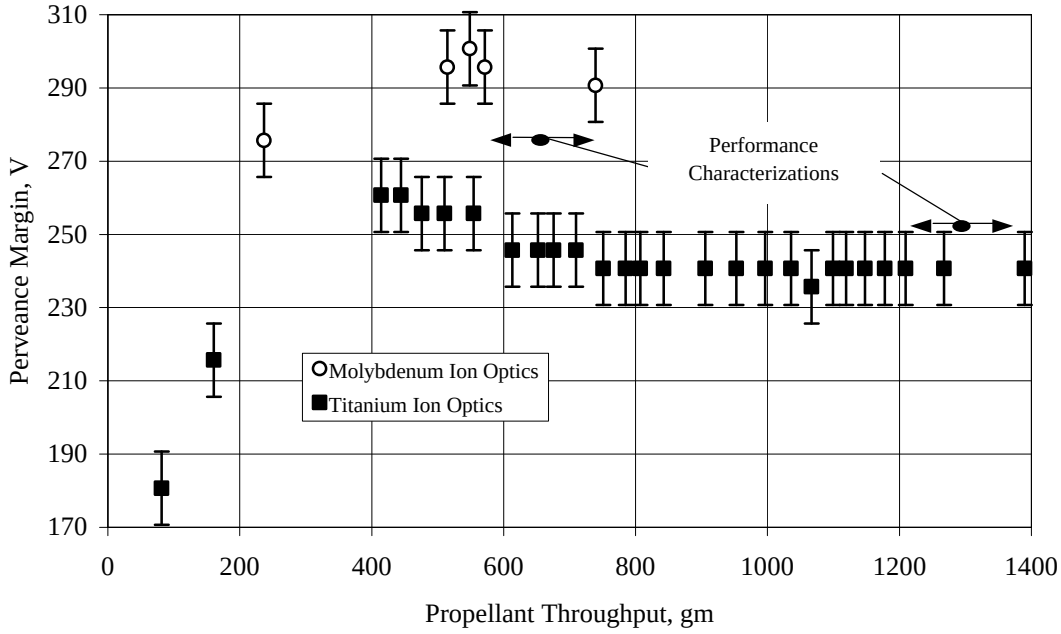

a. Perveance margin as a function of accumulated propellant throughput.

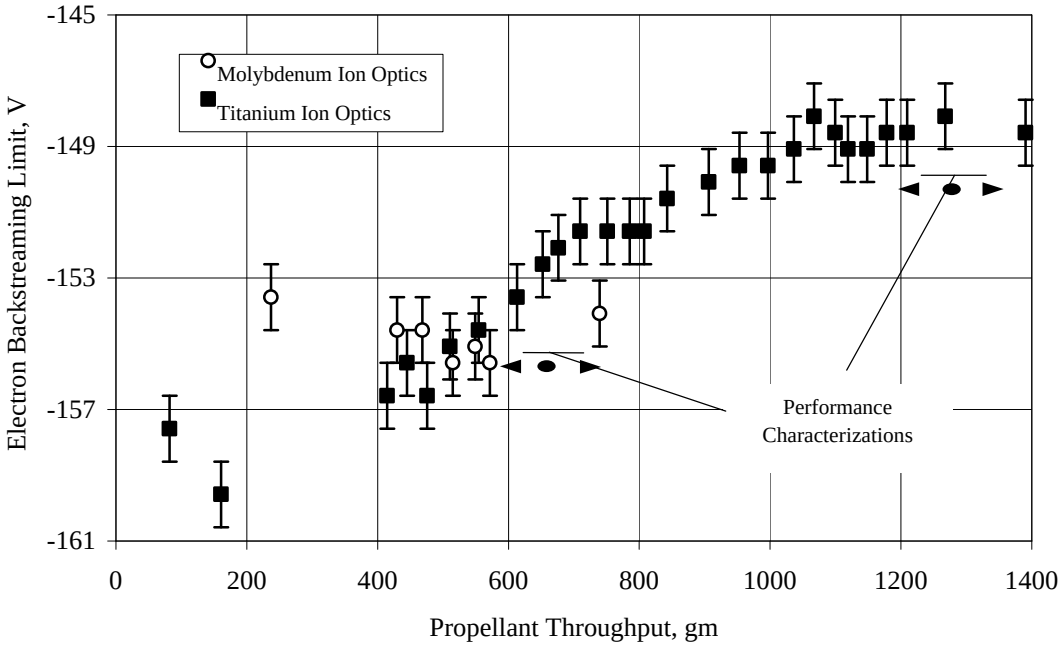

b. Electron backstreaming limit as a function of accumulated propellant throughput.

Fig. 3. Burn-in performance parameters at TH15 for titanium and molybdenum ion optics. (Continued)

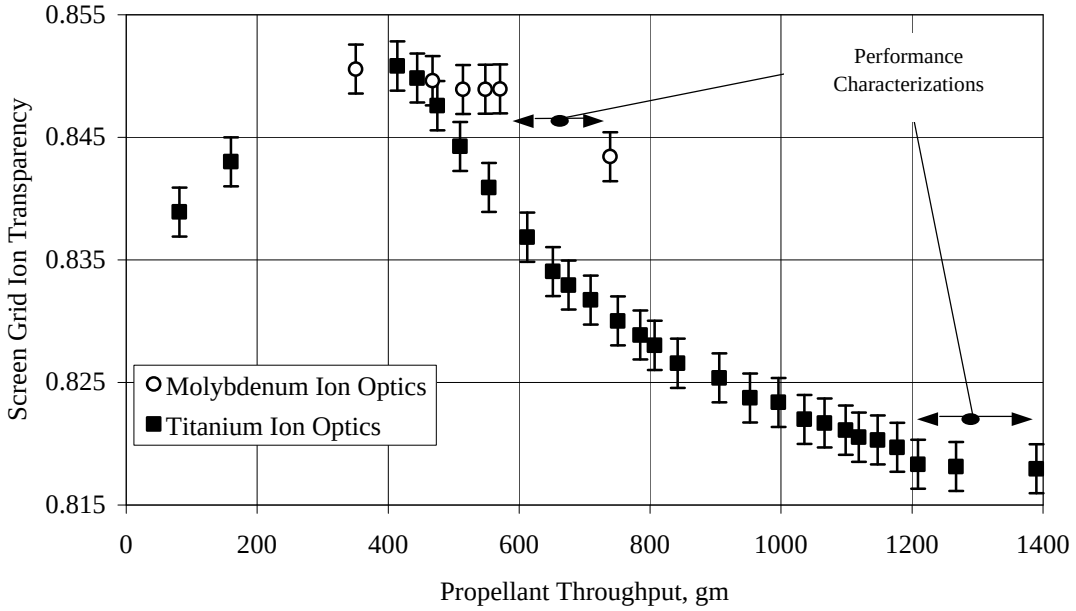

c. Screen grid ion transparency as a function of accumulated propellant throughput.

Fig. 3. Burn-in performance parameters at TH15 for titanium and molybdenum ion optics. (Concluded)

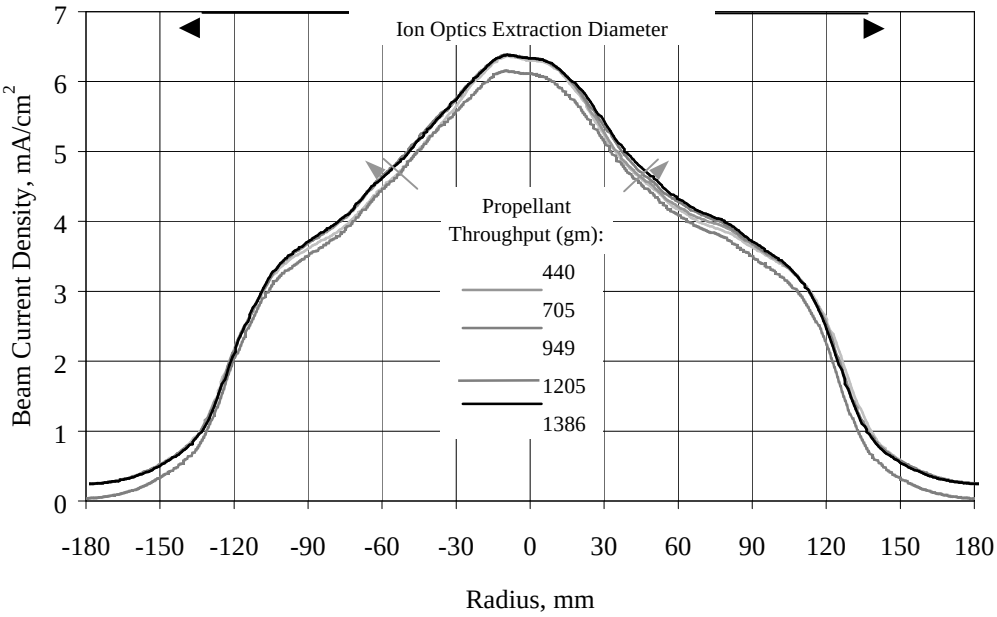

Fig. 4. Radial beam current density profiles for titanium ion optics during ion optics burn-in at various propellant throughputs. Profiles were measured 48 mm axially downstream of the grid center. Gray arrows indicate changes with accumulated propellant throughput.

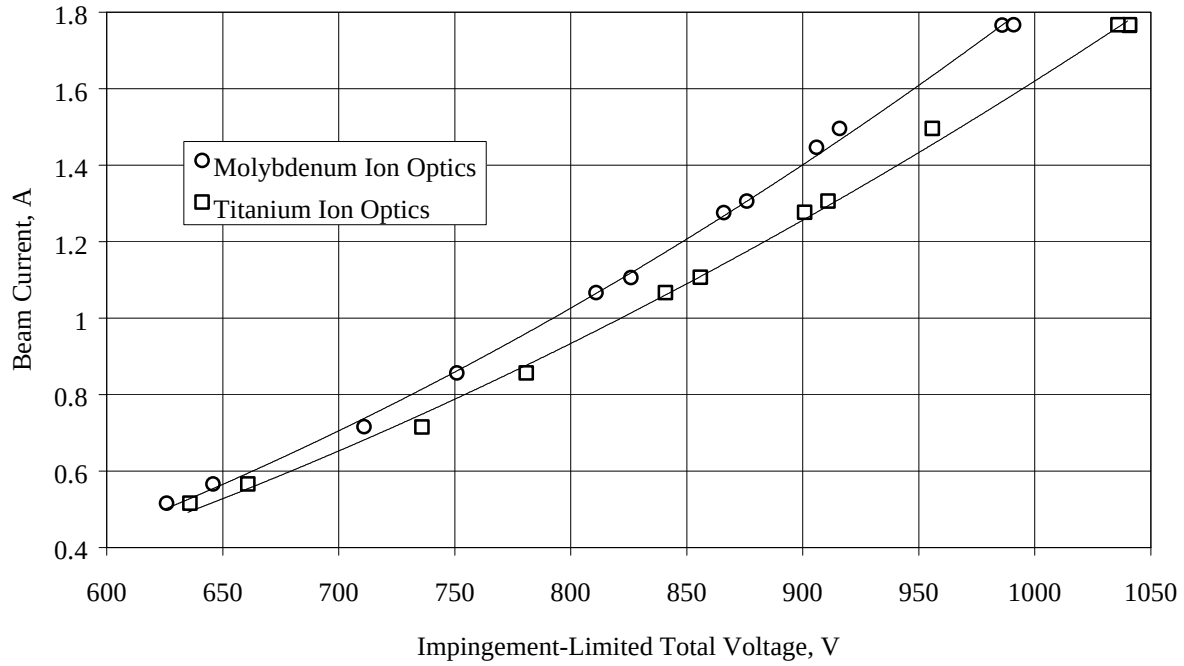

Fig. 5. Beam current as a function of impingement-limited total voltage for titanium and molybdenum ion optics.

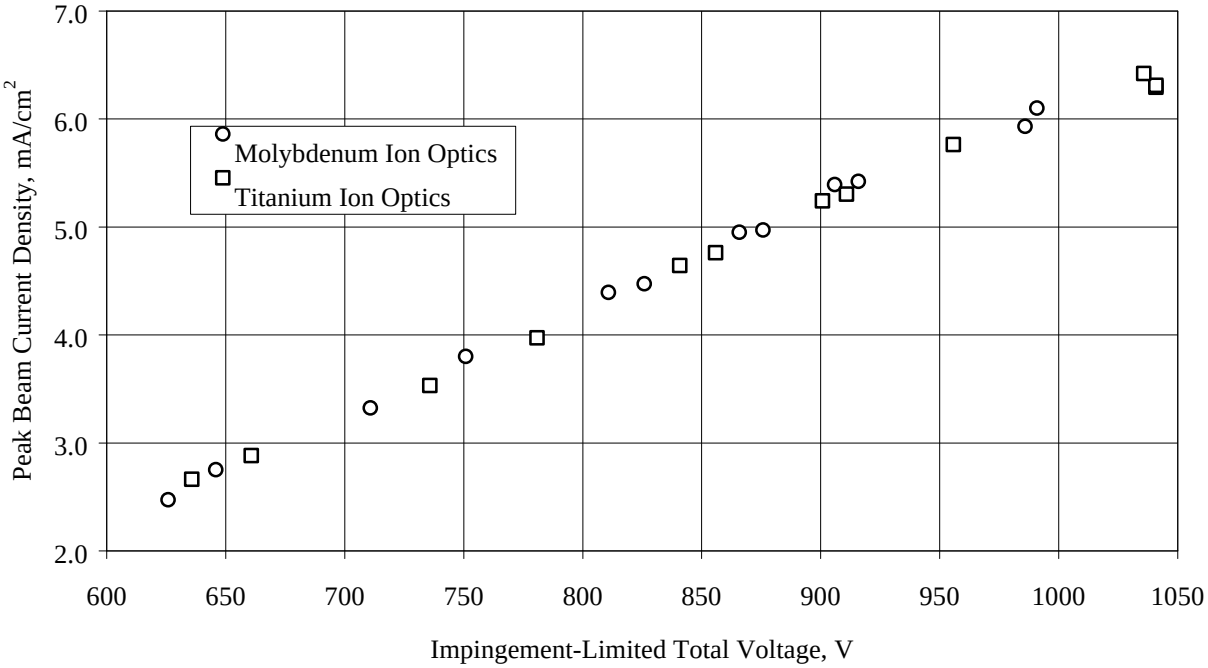

Fig. 6. Peak beam current density as a function of impingement-limited total voltage for titanium and molybdenum ion optics.

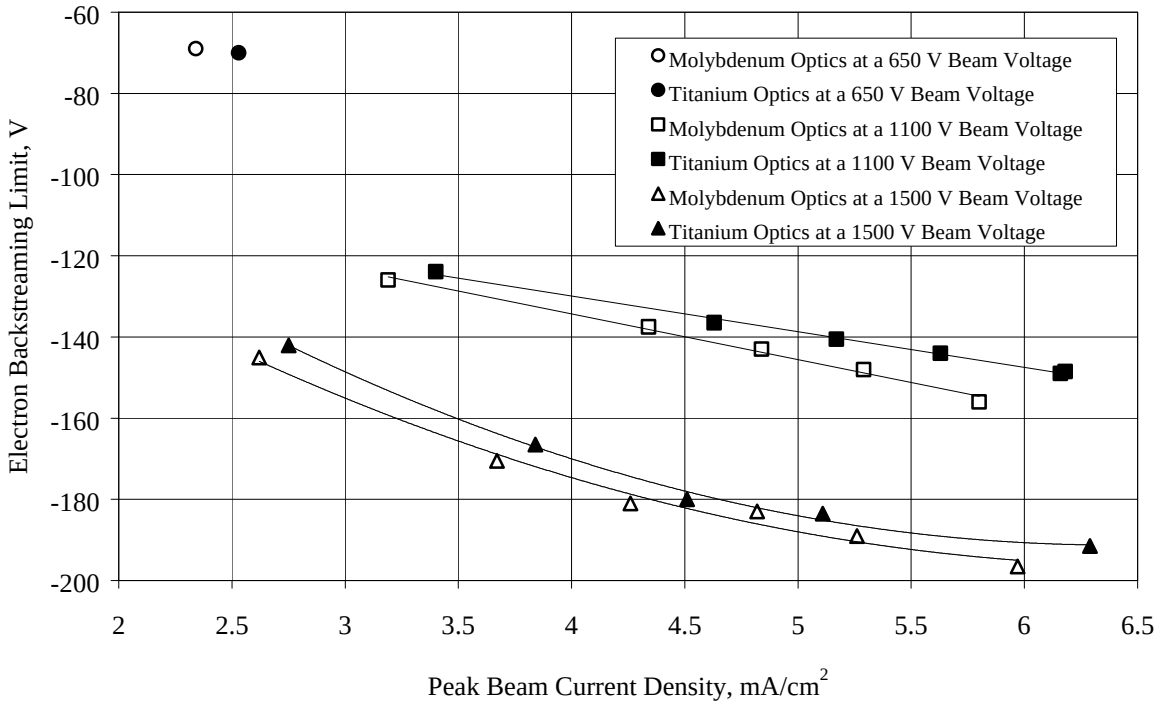

Fig. 7. Electron backstreaming limit as a function of peak beam current density for titanium and molybdenum ion optics. Peak beam current densities were measured 48 mm downstream of the ion optics' center. Beam voltages here are power supply voltages.

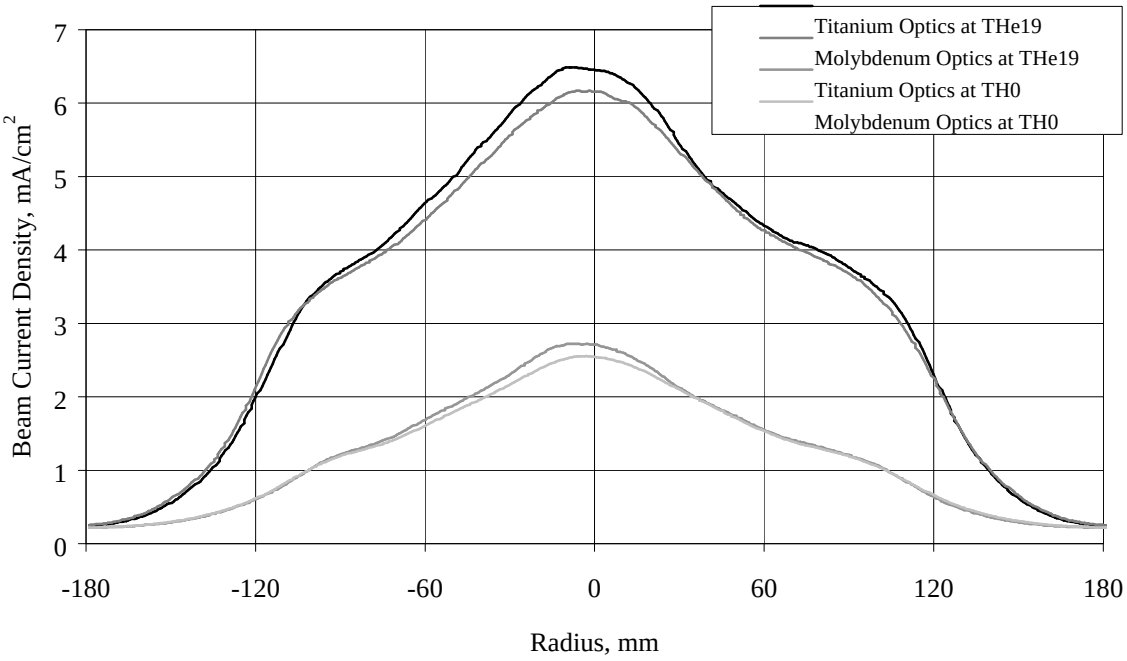

Fig. 8. Radial beam current density profiles for both titanium and molybdenum ion optics at THe19 and TH0. Beam current densities were measured 48 mm downstream of the ion optics' center.

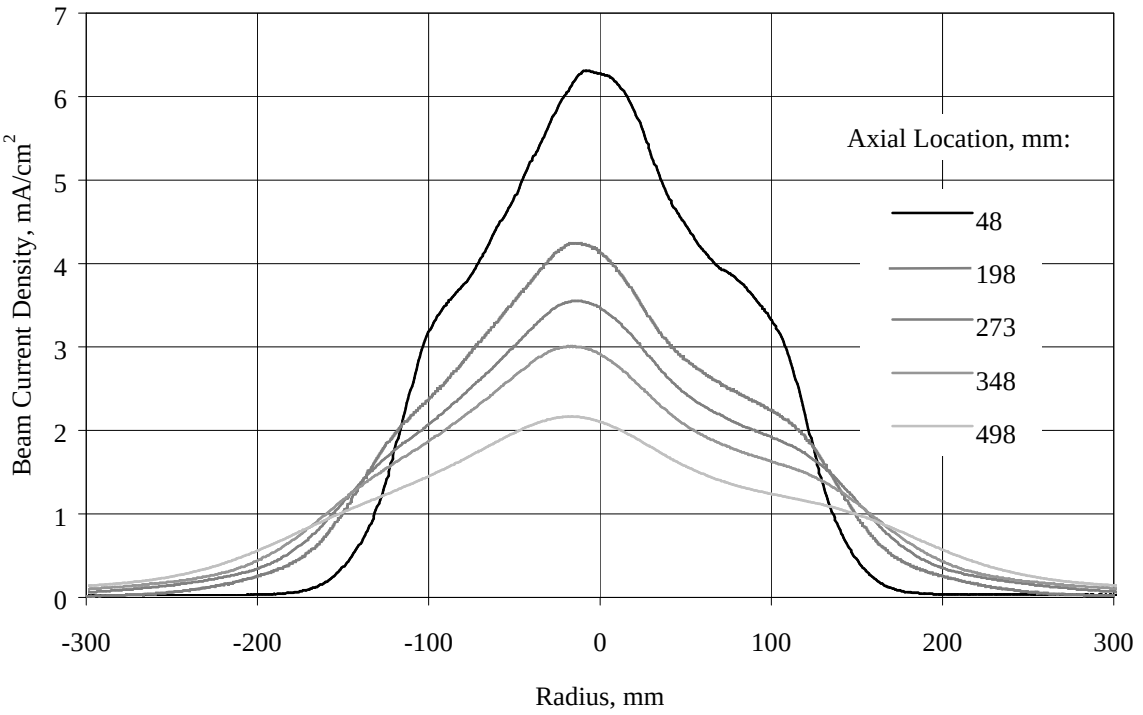

Fig. 9. Radial beam current density profiles at several axial locations for titanium ion optics at THe19.

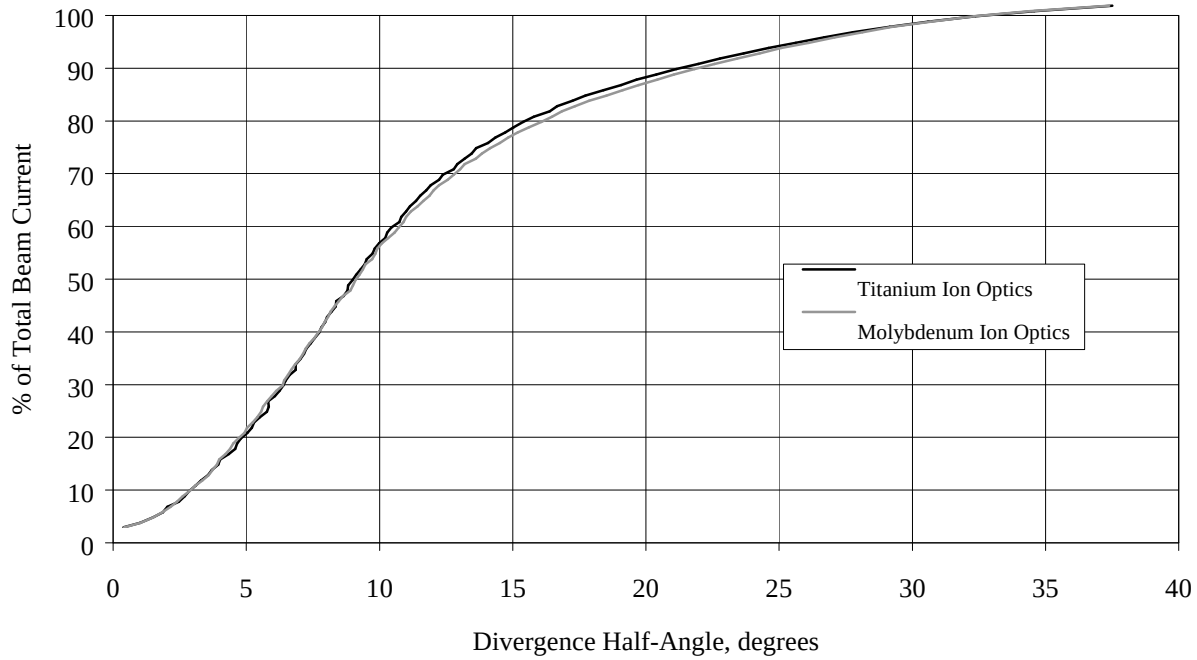

Fig. 10. Percentage of total beam current enclosed in a given divergence half-angle for both titanium and molybdenum ion optics at a THe19.